buildings

MDPI

Article

A Study of Composite Salt Erosion Resistance of Nano-Modified Cement Mortar in Early Ages

Jia Guo [1], Tao Zheng [1], Fei Mou [1], Yang Qin [1], Zhi Wang [1], Shiyi Zhang [2,*] and Hui Li [3]

[1] China Construction Third Engineering Bureau Group Co., Ltd., Wuhan 430014, China
[2] School of Civil Engineering and Architecture, Shandong University of Technology, Zibo 255000, China
[3] Zhongke Zhiyan (Shandong) Technology Development Co., Ltd., Linyi 273300, China
* Correspondence: zhangsy986@sdut.edu.cn

Abstract: Corrosion of traditional cement mortar is a critical issue in karst areas. Composite salt, i.e., sulfate–chloride salt, represents a typical corrosion agent due to the abundance of Cl^- and SO_4^{2-} ions in such geological environments. In this study, we used nano-metakaolin to enhance the physical and mechanical properties of cement mortar in the early aging stages, simulating groundwater corrosion by a compound salt solution in the karst region. The appearance and the change in the flexural/compressive strength of cement mortar upon the nano-metakaolin addition in the early aging stages under dry and wet cycling conditions were analyzed and combined with the results of scanning electron microscopy, thermogravimetric analysis, and other methods, revealing the underpinning mechanism behind the function changes of nano-metakaolin-modified cement mortar. The results show that nano-metakaolin effectively promotes cement hydration in the early aging stages. The flexural/compressive strength after 7 days of aging with 1% of added nano-metakaolin increased by 10.38% and 4.41%, respectively, compared to ordinary cement mortar. Furthermore, adding 1–5% of nano-metakaolin under dry and wet cycling and the coupling effect of chloride and sulfate erosion effectively reduce the damage of harmful ions on the cement mortar, leading to evident corrosion inhibition. The generation of hydration products increased after adding the Ghanaian metakaolin, filling the microcracks and micropores, and increasing the overall microstructural compactness.

Keywords: karst erosion; nano-metakaolin; cement mortar; chloride; sulfate

Academic Editor: Abdelhafid Khelidj

Received: 25 November 2024
Revised: 26 December 2024
Accepted: 16 January 2025
Published: 18 January 2025

Citation: Guo, J.; Zheng, T.; Mou, F.; Qin, Y.; Wang, Z.; Zhang, S.; Li, H. A Study of Composite Salt Erosion Resistance of Nano-Modified Cement Mortar in Early Ages. *Buildings* **2025**, *15*, 278. https://doi.org/10.3390/buildings15020278

1. Introduction

Karst exhibits unique geological characteristics, and it is widely distributed in southwest and south China. Such geological localities are prone to exceptional degradation stress and possess a complex underground water system, which, altogether, challenge engineering construction. Recent technological and machinery-related advancements have fostered the construction of high-speed railways and tunnels through karst formations. However, the well-developed water system and high salt concentration (such as chlorides and sulfates) in karst regions inevitably influence the corrosion resistance and durability of high-speed railways and tunnel concrete constructions, gradually affecting the long-term stability [1–4]. The groundwater corrosion of concrete structures mainly originates from Cl^- and SO_4^{2-} salts, and traditional cementitious materials with poor mechanical properties and durability cannot meet the engineering requirements in the harsh environment of karst areas [3–6].

Nanotechnology has found a great application milieu in the construction industry as an essential part of the frontier field [7,8]. Various nanomaterials are commonly used for

modifying cement-based materials, such as nano-SiO_2 (NS) [9], nano-$CaCO_3$ (NC) [10], carbon nanotubes (CNTs) [11], graphene, and nano-clay. Among them, nano-clay contains nano-kaolin, which is easily obtained, inexpensive, and environmentally friendly compared to other nanomaterials. Moreover, it possesses excellent physical and chemical properties, such as a nucleation-induced hydration reaction and volcanic ash effect, and can enhance and improve the performance of cement-based materials [12–14]. Therefore, applying nano-metakaolin as a replacement for some cement components has become a research hotspot in construction materials.

Chen et al. [15] reported that nano-metakaolin micro-aggregates successfully filled the pores between cement particles and promoted hydration. It reacts with $Ca(OH)_2$ (CH) to produce calcium silicate (C-S-H) gel via a volcanic ash reaction, which can fill the pores and cracks inside the cementitious material, thus forming a dense microstructure and hindering chloride ion in-diffusion and sulfate erosion. Althoey et al. [1] investigated the hydration of a cement paste with nano-metakaolin, finding that nano-metakaolin can promote the formation of the internal structure of the cement paste in the early hydration period. Similarly, Maohua et al. [16] found that nano-metakaolin can regulate the cement hydration process and promote the early hydration reaction due to its nucleation effect while improving the compactness of the internal structure. Mokhtar et al. [17] and Raza et al. [18] investigated the effect of nano-metakaolin on the mechanical properties, chloride ion penetration resistance, and sulfate erosion of concrete and cement mortar in an erosive environment. Metakaolin significantly increased the compressive and flexural strength of concrete and cement mortar, and, at the same time, strongly enhanced their resistance to chloride penetration and sulfate erosion. Nevertheless, most studies on concrete erosion in the tidal zone focus on the later stage of concrete damage, while only a few studies have assessed the early stage of a concrete degradation process [18–21], although it is irreversible and affects the entire concrete life cycle.

In this paper, cement mortar is used as the object of study. The dry and wet cycling system simulates the corrosion process of salt solution in the karst area. It investigates the erosion behaviour of the chloride–sulfate mixed solution by dry and wet cycling on the cement mortar with nano-metakaolin at an early age. The effects of nano-metakaolin on the properties of cement mortar were investigated in terms of changes in appearance, morphology, and quality, as well as changes in mechanical properties. According to the scanning electron microscope (SEM) and thermogravimetric (TG) analysis of its microstructural characteristics and changes in the content of the physical phase components, the influence of nano-metakaolin on the hydration rate and corrosion resistance of cement mortar was analyzed. Theoretical support is provided for the application of nano-metakaolin in the modified cementitious material.

2. Materials and Methods

2.1. Materials

The following materials were used in the study: P-O42.5 ordinary silicate cement produced by Shanshui Dongyue as test cement, class I fly ash, and nano-metakaolin supplied by Wuhan (China) Huashen Intelligent Energy Science and Technology Company Limited, the compositions of which are shown in Table 1. The particle size distribution of nano-metakaolin is shown in Figure 1.

Table 1. Chemical composition.

Chemical Composition	CaO	SiO_2	Al_2O_3	Fe_2O_3	MgO	SO_3	K_2O	Na_2O
Cement content/%	59.31	21.90	6.26	3.79	1.63	2.41	-	-
Fly ash content/%	3.16	53.80	24.60	9.32	1.52	-	0.82	0.28
Nano-metakaolin content/%	0.10	46.28	50.46	0.44	0.13		0.11	0.26

Note: The "%" in the article refers to the ratio to the total weight.

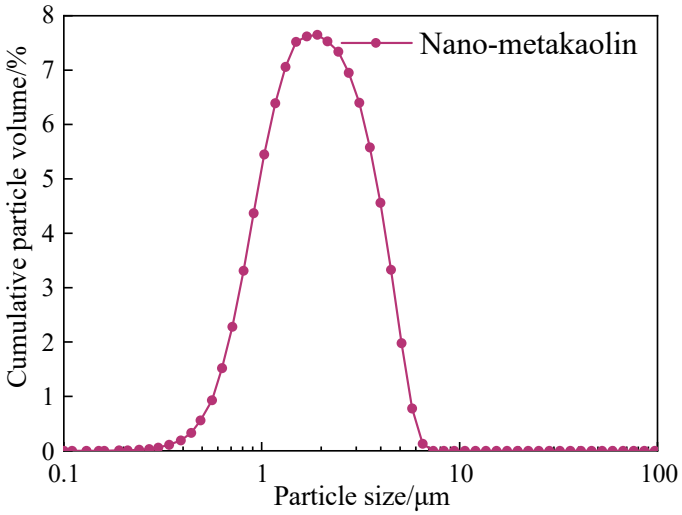

Figure 1. Particle size distribution of nano-metakaolin.

2.2. Test Specimen Mixing Ratio and Production

Test specimen ratios and test groups are shown in Tables 2 and 3, respectively.

Table 2. Specimen mixing ratios.

Specimen Number	Cement/g	Fly Ash/g	Nano-Metakaolin Clay/g	Sand/g	Water/g
7A	315	135 (30%)	0	1350	225
7B	310.5	135 (30%)	4.5 (1%)	1350	225
7C	292.5	135 (30%)	22.5 (5%)	1350	225
7D	270	135 (30%)	45 (10%)	1350	225

Table 3. Experimental groupings.

Specimen Number	No Wet/Dry Cycle	Dry and Wet Cycle for 30 Days	Dry and Wet Cycle for 60 Days
7A	7A00	7A30	7A60
7B	7B00	7B30	7B60
7C	7C00	7C30	7C60
7D	7D00	7D30	7D60

Note: 7A, 7B, 7C, and 7D are different-mix-proportion groups for 7 days of maintenance, and the details are shown in Table 2.

A prismatic cement mortar specimen with a size of 40 mm × 40 mm × 160 mm was used in this test. When making the specimens, the weighed nano-metakaolin and water were mixed and put into an ultrasonic disperser for efficient dispersing. After that, cement, fly ash, mixing solution, and standard sand were poured into a cement mortar mixer for thorough mixing. The mixed cement mortar is poured into the mold for full vibration. The

mold was removed after 24 h of resting after pouring and then put into a standard curing room with (20 ± 2 °C) and a relative humidity of more than 95% for curing. Details on the preparation procedure are shown in Figure 2.

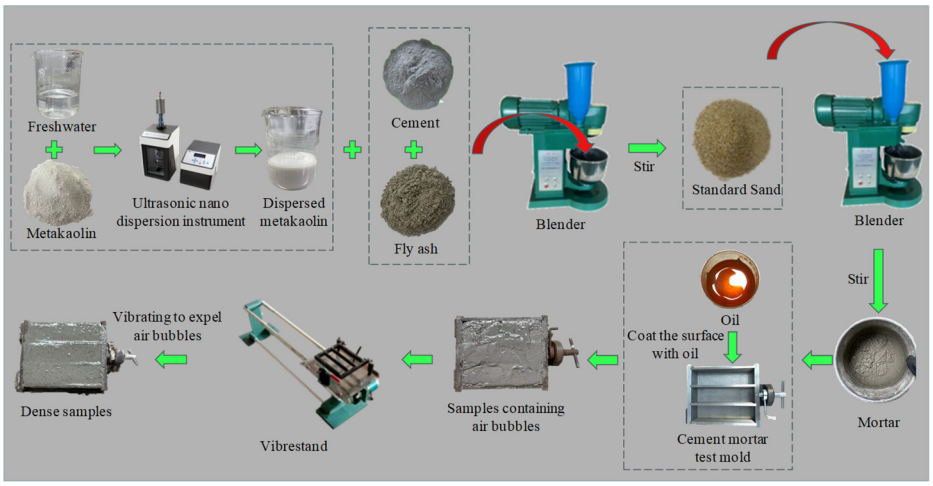

Figure 2. Preparation process of specimen.

2.3. Test Methods and Procedures

2.3.1. Corrosion Methods

The change in the groundwater level in the karst area was simulated based on the time law of groundwater rise and fall. Corrosion tests were carried out using a dry and wet cycle immersion system following a sequence of 6 h of immersion and 6 h of ventilated drying at room temperature, with two sets of cycles per day. The corrosion solution comprised 10% Na_2SO_4 and 5% NaCl [22].

The corrosion test steps are as follows:

(1) Before starting the experiment, all specimens must be pre-treated (e.g., surface cleaning, dimensional measurement, etc.) according to the experimental requirements, and then we record the initial state.

(2) The specimens are fully immersed in the pre-configured corrosion solution for 6 h. It must be ensured that the solution fully covers the specimen; the setup must be inspected periodically to prevent concentration changes due to the solution evaporation.

(3) After removing the specimen from the solution, the specimen is allowed to dry at room temperature for 6 h under ventilation by a fan or other means to accelerate air circulation. Direct blowing onto the specimen must be avoided to avoid unnecessary stress.

(4) The above wet–dry cycle is performed twice a day; i.e., two complete soaking–drying cycles are completed in one day. To ensure stable solution concentration, the corrosion solution is replaced every 7 days.

2.3.2. Physical Appearance and Quality Changes

After removing the specimens from the corrosion solution, the surface moisture was dried with a towel, and the macroscopic appearance was photographed and recorded after natural air drying for 6 h. The visual changes of the cement mortar specimens were evaluated from several aspects, such as surface smoothness, number of holes, diameter, and integrity at the corners. At the same time, the specimen mass was weighed, and the relative mass change rate was calculated.

2.3.3. Mechanical Performance Test

Mechanical properties tests were conducted in accordance with the "cementitious sand strength test method" (GB/T17671-2021 [23]) standard. Prismatic specimens with a size of 40 mm × 40 mm × 160 mm were used. Groups consisting of 3 specimens were removed after 7 days of curing and after completing a specific time of wet and dry cycles, and were subjected to flexural and compressive tests.

2.3.4. SEM

An Apreo field-emission scanning electron microscope (FEI, Hillsboro, OR, USA) was used to observe the microscopic morphology of the test samples. To obtain clearer and more realistic SEM images, specimens were dried and cut, and the surface was gold-sputtered before measurement to improve the conductivity. The ambient temperature during measurement was 20 °C.

2.3.5. TG/DSC

The prepared powder samples were analyzed using a thermogravimetric analyzer (TA Instruments, Shanghai, China) in the temperature range from 30 to 1000 °C, with a heating rate of 10 °C/min. The whole heating was conducted in a protective nitrogen environment with an airflow rate of 50 mL/min. $Ca(OH)_2$ calculations were made referring to the literature [19].

3. Results and Discussion

3.1. Changes in the Appearance and Quality

As shown in Figure 3, the surface of the cement mortar specimen without salt solution corrosion is relatively smooth and grey, without flaking on the mortar surface and with sharper surface pores. The specimen's surface whitens as the duration of the wet and dry cycles increases. At the same time, the mortar surface shows an apparent flaking phenomenon, and the aggregate is exposed at the corners. The surface is very rough, and the surface pores are more rounded after erosion by the salt solution, accompanied by precipitation of white needles and rod crystals.

Figure 4 shows that the mass of each group roughly increases and then decreases with the duration of dry and wet cycles. The reason for this is that, in the early stage of aging, the cement hydration reaction of each group still proceeds; i.e., the hydration products are continuously generated, and the overall quality of the specimens improves. After the cement hydration reaction is completed, the erosion of the specimen by the salt solution is gradually revealed on the macroscopic level due to the accelerating effect of dry and wet cycling. Thus, the surface flaking phenomenon of different degrees leads to a more obvious quality decline. However, the trend of the relative mass loss rate of each group of specimens tends to level off with the wet–dry cycling duration, plausibly due to the secondary hydration of chloride and sulfate ions into the internal cavities, such as micropores or microcracks, of the specimens, compensating, to a certain degree, the mass loss caused by the surface erosion by the corrosive solution [24].

Figure 3. Changes in appearance and morphology of different nano-metakaolin without wet/dry cycling and wet/dry cycling for 30 d.

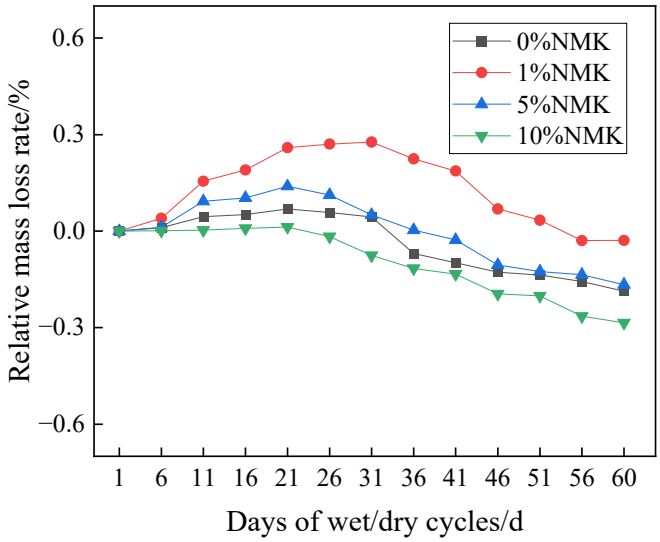

Figure 4. Relative mass loss rate of each group with increasing days of wet and dry cycling after 7 d of curing.

Regarding the nano-metakaolin dosage, the hydration of cement with 1 and 5% of added nano-metakaolin is favorable, i.e., better than for the cement without additive. However, the hydration effect of cement containing 10% of nano-metakaolin is less satisfactory, probably due to the high number of nano-metakaolin particles, which triggers the agglomeration effect and, thus, inhibits the rate of cement hydration [25].

3.2. Effect of Nano-Metakaolin Dosing on Mechanical Properties

Figure 5 shows the effect of the nano-metakaolin dosage on the flexural and compressive strength of cement mortar specimens without wet and dry cycles. The initial

strengthening and then weakening occur with the increase in nano-metakaolin dosage, being the highest when the dosage of nano-metakaolin is 1% and the lowest without nano-metakaolin. Figure 5b shows that the flexural and compressive strength values of specimens doped with 1% nano-metakaolin increase by 10.38 and 4.41%, respectively, compared to the control sample without nano-metakaolin. Remarkably, the flexural and compressive strength values of specimens doped with 10% of nano-metakaolin are less increased, only by 3.63% and 0.75% relative to the control.

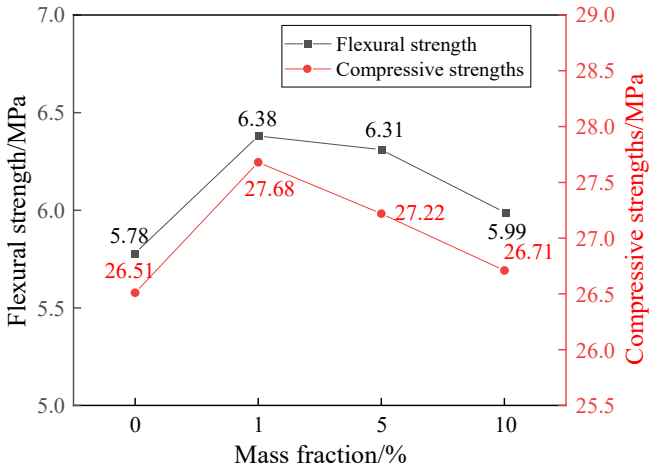

(**a**) Flexural and compressive strengths

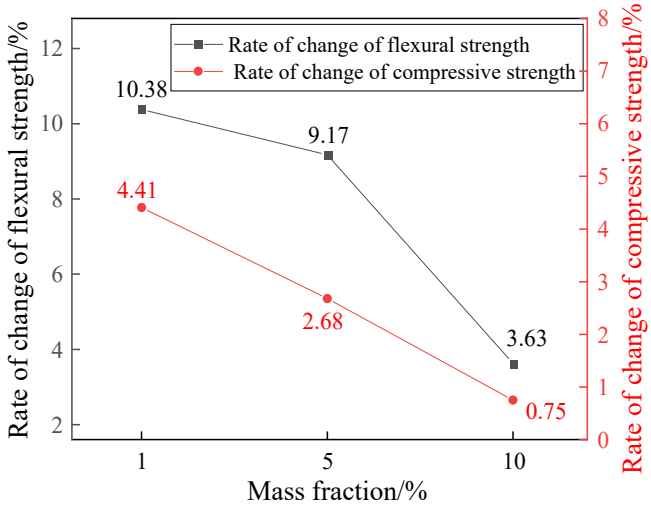

(**b**) Rate of change of flexural compressive strength

Figure 5. Effect of nano-metakaolin dosing on flexural compressive strength without dry–wet cycling.

Figure 6 depicts the effect of nano-metakaolin dosing on the flexural and compressive strengths upon 30 d of wet and dry cycling. The flexural and compressive strength values of each group change following a similar trend as before conducting wet and dry cycling, showing the initial strengthening and then weakening with the increase in the nano-metakaolin content. The highest strength of the specimens appears for a nano-metakaolin dosage of 1%, and the flexural and compressive strengths increase by 5.42 and 2.42%, respectively, compared with the control group. When the dosage is 10%, the strength values are the lowest, being even lower than those of the undoped nano-metakaolin group; i.e., the flexural and compressive strengths are decreased by 4.23 and 1.03%, respectively, compared to the control group. This can be observed by looking at Figures 5b and 6b. The increase in the rate of change in strength at the age of 7 d is greater compared to the rate of change in

strength at the age of 7 d followed by 30 d of wet and dry cycling. This indicates that the doping of Ghanaian rice metakaolin promotes cement hydration at an early age of cement mortar to some extent.

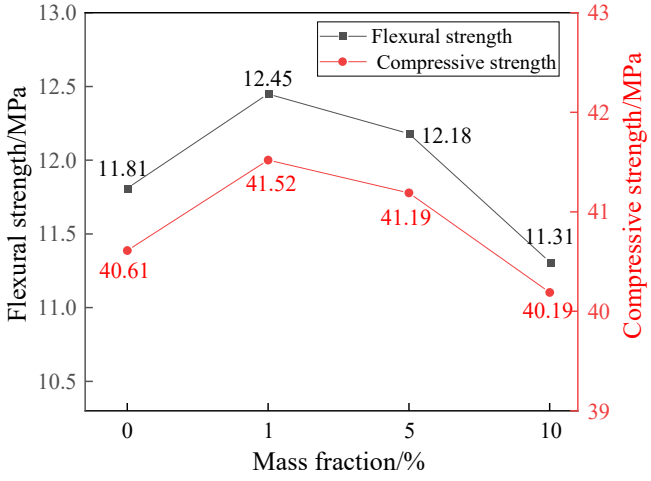

(**a**) Flexural and compressive strengths

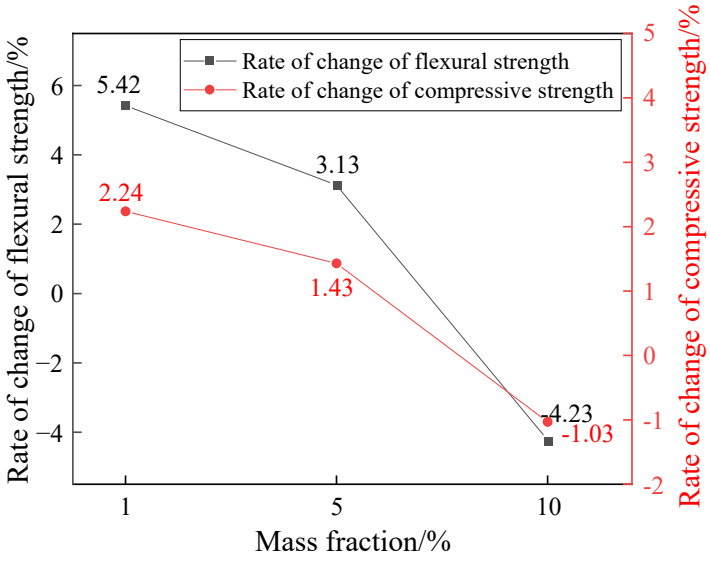

(**b**) Rate of change of flexural compressive strength

Figure 6. Effect of nano-metakaolin dosing on flexural compressive strength at 30 d of wet and dry cycling.

3.3. Effect of Nano-Metakaolin Dosing on the Hydration Process of Cement

3.3.1. Microstructure

The microstructure of ordinary cement mortar during the cement hydration process was examined in the early aging stages (Figure 7). The generation of CH in the sample is relatively small, the hydration rate is slow, and there are still many unhydrated cement particles; the number of pores and cracks is large, and the overall compactness of the microstructure is poor. In the sample containing 1% of nano-metakaolin, the amount of hydration products is somewhat higher than that for the control. The C-S-H gels mainly appear in the form of amorphous irregularly clustered particles. It is also accompanied by a small number of CH crystals, a reduced number of pores, better wrapping around fly ash (FA) particles, and tight interfacial bonds, which effectively improve the microstructure of the mortar matrix. In addition, a few acicular calcovanadite (AFt) crystals are formed in

the pores, resulting in a uniform and tight distribution of hydrated particles and a denser overall microstructure than in the control group. In the cement samples containing 5% of nano-metakaolin, the C-S-H gel distribution is more concentrated than for the specimens doped with 1% of nano-metakaolin. The number of plate-like CH crystals in the samples is significantly reduced, a higher amount of C-S-H gel is formed, and spherical fly ash particles are embedded in the C-S-H gel lattice. At the same time, the C-S-H gel parcel covers the CH and AFt crystals, restricting the available space, which improves the microstructure of the mortar matrix to a certain extent, although it is more porous compared to the 1% nano-metakaolin sample. The cement sample containing 10% of nano-metakaolin exhibits more pores and a larger pore size. The particles are loosely lapped, with loose connections between the hydration products, and the hydration degree is lower than that of the samples doped with 1 and 5% of nano-metakaolin.

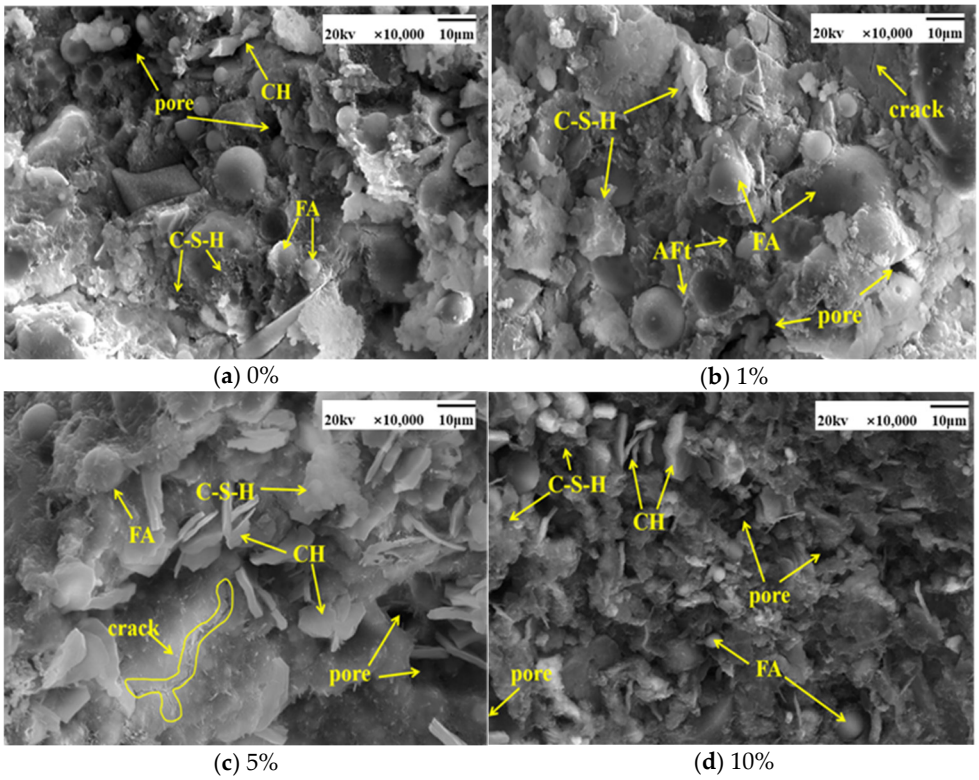

Figure 7. SEM scanning electron microscope images of different nano-metakaolin dosages without wet/dry cycling.

Figure 8 shows SEM images of samples with different nano-metakaolin dosages after 30 d dry and wet cycles. For the samples without nano-metakaolin, the cement mortar is tightly bonded, but the matrix shows large cracks. During the dry and wet cycling process, chloride and sulfate ions in the solution enter the specimen's interior through the cracks, thus affecting the strength of the cement mortar. The overall structure of the sample with 1% of nano-metakaolin is denser and better bonded, and the number of microcracks and micropores is significantly reduced. Fly ash particles are tightly wrapped, and the C-S-H gel amount is increased after secondary hydration. The number of hydration products in the sample increases with a nano-metakaolin dosage of 5%. Friedel's (Fs) salt is produced, blocking the channels for the penetration of harmful ions; the overall morphology is denser, but some pores and cracks still exist. In the sample with 10% of nano-metakaolin, the number of internal pores and holes is significantly increased, forming penetrating cracks. At the same time, the matrix surface is no longer flat and becomes uneven, resulting in a significant strength reduction [26].

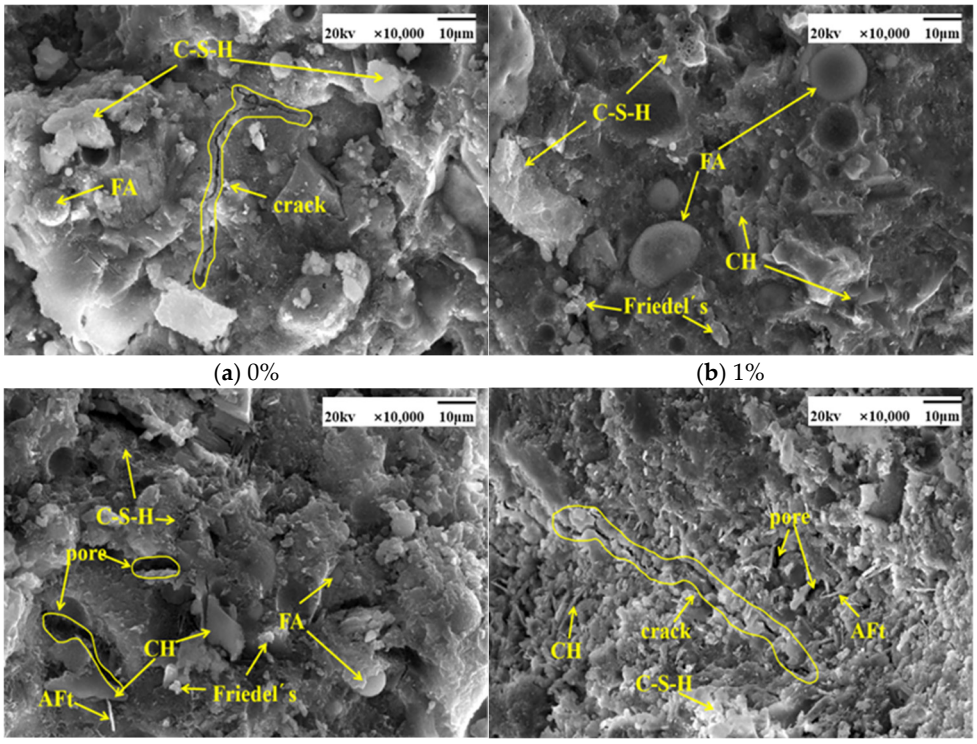

(**a**) 0% (**b**) 1%

(**c**) 5% (**d**) 10%

Figure 8. SEM scanning electron microscope images of different nano-metakaolin dosages in dry and wet cycling for 30 d.

3.3.2. Thermogravimetric Analysis

The TG/DSC histograms at different nano-metakaolin dosages without drying and wetting and the $Ca(OH)_2$ (CH) content at different nano-metakaolin dosages without drying and wetting are shown in Figures 9 and 10, respectively. The content of CH crystals inside the nano-metakaolin cement mortar is higher than that of the standard cement mortar without dry and wet cycling. The nano-metakaolin cement mortar with a 1% dosage has the highest number of internal CH crystals, i.e., 32.52% higher compared to ordinary cement mortar. Cement mortar samples with a 5 and 10% nano-metakaolin dosage also show an increase of 6.08 and 5.17%, respectively, compared to ordinary cement mortar. Meanwhile, the C-S-H gel decomposition peaks of the nano-metakaolin-doped cement mortar are more profound than those of the ordinary cement mortar, indicating that nano-metakaolin particles can effectively promote cement hydration in the early aging stage.

The TG/DSC histograms at different nano-metakaolin dosages and the $Ca(OH)_2$ content are shown in Figures 11 and 12, respectively, upon the exposure to wet and dry cycles for 30 d. After 7 d of curing and 30 d of wet/dry cycling, the sample doped by 1% of nano-metakaolin has the highest number of CH crystals inside the cement mortar, 16.44% higher compared to the ordinary cement mortar. At 5 and 10% of nano-metakaolin cement mortar dosages, 3.01 and 29.63% fewer CH crystals appear than for ordinary cement mortar. The C-S-H gel decomposition peaks of the cement mortars with 1 and 5% of nano-metakaolin mortars are more profound than those for ordinary cement mortars after 30 d of wet and dry cycling at 7 d of curing. This may occur because nano-metakaolin exerts its volcanic ash effect, which can generate an additional hydrated C-S-H gel by the secondary reaction with CH. The decrease in the CH content of the 5% nano-metakaolin-doped cement mortar may be due to the faster secondary reaction, which consumes more CH and, thus, generates more C-S-H gel.

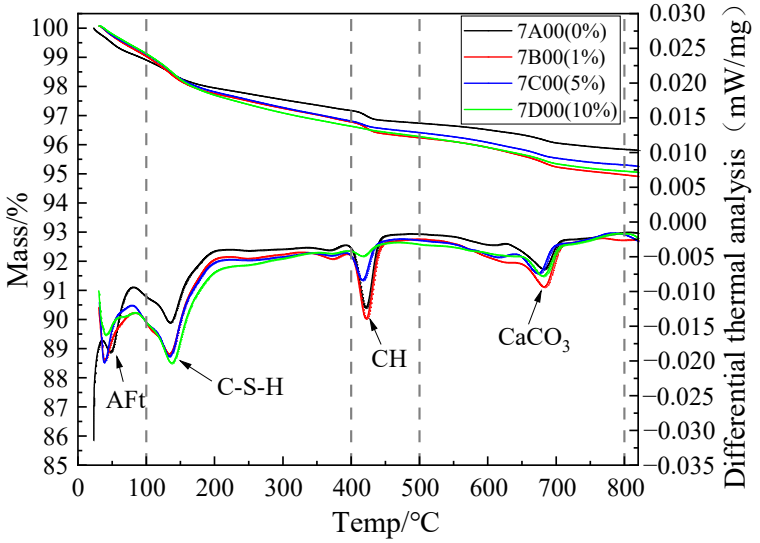

Figure 9. TG/DSC for different nano-metakaolin dosage without drying and wetting.

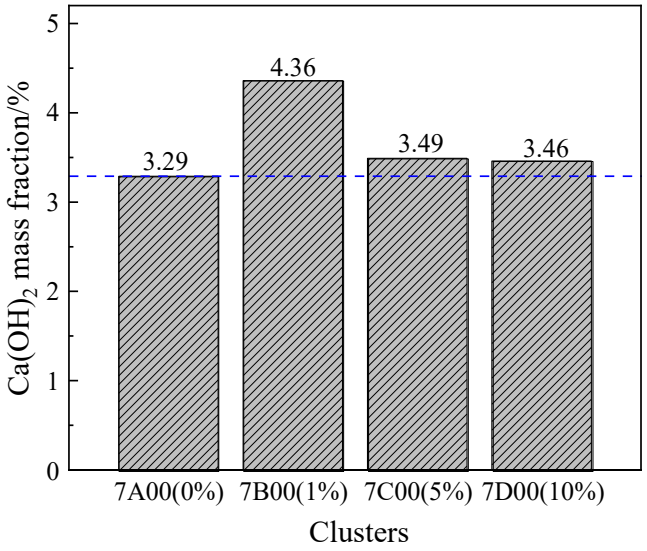

Figure 10. Histogram of $Ca(OH)_2$ content of different nano-metakaolin dopings when not wet or dry.

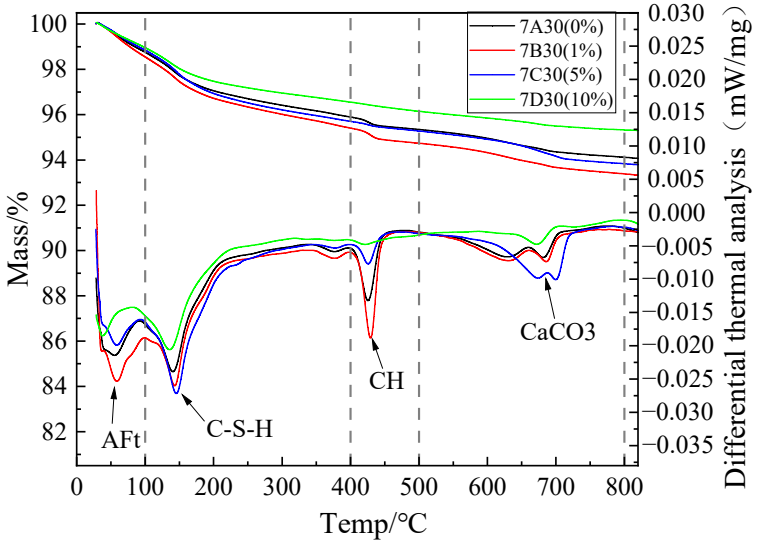

Figure 11. TG/DSC at 30 times of dry and wet with different nano-metakaolin dosages.

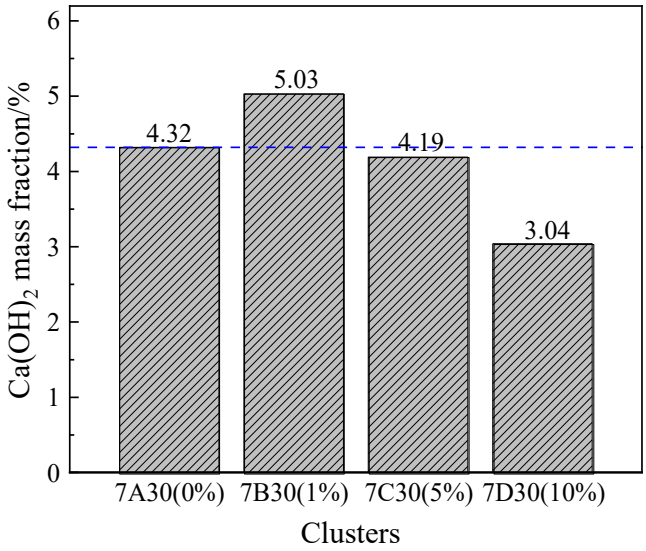

Figure 12. Histogram of $Ca(OH)_2$ content with different nano-metakaolin dosages at 30 d of dry and wet cycling.

In contrast, the C-S-H gel decomposition peak of the 10% nano-metakaolin-doped cement mortar is weaker than that of ordinary cement mortar, which may be due to the small size of nano-metakaolin, yielding a higher surface energy. As the nano-metakaolin dosage increases, the agglomeration effect occurs between the particles, inhibiting the later cement hydration.

3.4. Degradation of Cement Mortar Pore Structure Under Dry–Wet Cycle–Complex Salt Action

The above analysis shows that the 5% nano-metakaolin-fly-ash-based cement mortar specimen exhibits better mechanical properties and microstructural characteristics when resisting the action of dry and wet cycling and composite salt. Since the size of the internal pore structure parameter of cementitious materials is one of the main reasons relevant for the penetration of aggressive ions, the integral and differential distribution curves of pore sizes of the specimens of groups 7C00, 7C10, 7C30, and 7C60 with different depths from the mortar surface are determined by MIP (Figure 13), to reveal the mechanism of the dry and wet cycling effects on the pore structure of the nano-metakaolin-modified fly ash cement mortar.

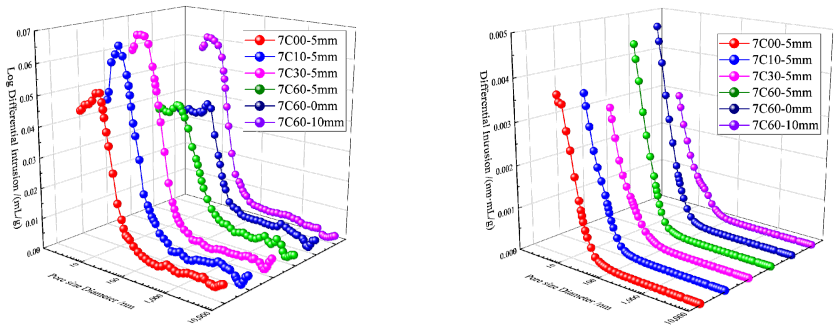

(**a**) Differential curve of aperture distribution (**b**) Aperture distribution integral curve

Figure 13. Pore diameter distribution curve of cement mortar.

According to Wu's classification method [27], the cement's pore structure can be categorized into four types based on the pore size range. The results obtained by comparing the specific pore volume of each pore size range and its percentage in the total specific

pore volume are shown in Table 4, and the pore size distribution histogram is shown in Figure 14.

Table 4. Pore size distribution of cement pastes.

	7C00-5 mm/%	7C10-5 mm/%	7C30-5 mm/%	7C60-5 mm/%	7C60-0 mm/%	7C60-10 mm/%
Much harmful pores	0.2	0.24	0.21	0.37	0.41	0.16
Harmful pores	3.58	3.32	2.17	6.73	6.73	2.39
Little harmful pores	25.39	25.12	20.42	20.74	22.31	20.45
Harmless pores	70.81	71.3	77.18	72.14	70.53	76.98

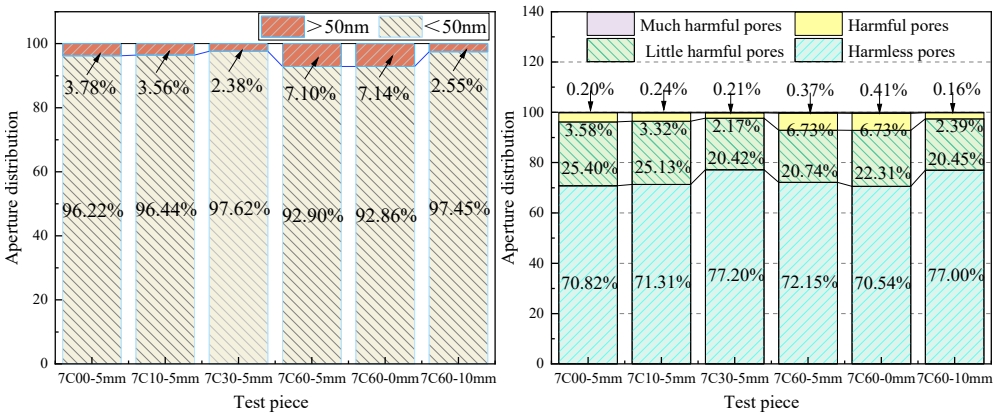

(**a**) (**b**)

Figure 14. Percentage of each level aperture to total specific pore volume: (**a**) 50 nm critical pore size as a percentage of total pore volume; and (**b**) four types of holes.

It can be obtained from the data in Table 4 and Figure 14. With the increase in the duration of wet and dry cycling, the number of harmless and less harmful pores in cement gradually increases at the cost of polypores and harmful pores. Eventually, the percentage of harmful pores and polypores is decreased by 47% after 60 wet and dry cycles, and both pore size distributions shift toward the smaller pore size range. The hydration process of cement continues, and the hydration products fill the internal pores of cement mortar. The reduction in the capillary pore volume and pore connectivity in cement mortar prevents aggressive ions from entering the interior of the cement mortar, improving the pore structure. The cement mortar is mixed with MK, whose micro-aggregate and volcanic ash reactions refine the cementitious material's pore structure and improve the pore structure's compactness. The Friedel salt generated by the chloride ions preferentially enters the specimen's interior and reacts with minerals such as C_3A, which can fill in the large pores, refining the pore size and limiting the generation of swelling erosion products such as AFt after the intrusion of sulfate ions.

By comparing the pore distribution of specimens with different depths in group 7C60 (0 mm, 5 mm, and 0 mm), it can be found that the number of harmful and multi-harmful pores gradually decreases with the increase in the depth of cement mortar. Due to the short curing age of cement mortar, the cement mortar is practically just molded, and the hydration reaction of cement requires the absorption of a large amount of water, and, with that, many chloride and sulfate ions from the external environment are brought into the cement mortar. However, the transport of the sulfate and chloride ions from the surface layer into the depth of the cement mortar is hindered due to the slow diffusion, leading to their accumulation in the surface layer, which exacerbates the erosion of the surface layer and leads to the sanding of the surface layer [28]. At the same time, this also introduces a

constraining effect on chloride and sulfate ions. With few wet and dry cycles, no erosive damage appears in the deeper layers of cement mortar.

Figures 15 and 16 illustrate the characteristic parameters of the internal pore structure and the porosity of nano-metakaolin mortar at different durations of dry and wet cycling, respectively. After 60 d of wet and dry cycling, the most available pore size and the total specific pore size at the same depth (5 mm) first decrease and then increase. Analyzing only the change in the depth of the 7C60 group, the most prominent pore diameter and the total specific pore volume gradually decrease. Moreover, at 0 mm, the most abundant pore size is 26.295 nm, which falls within the range of less harmful pores. Moreover, the internal cement mortar layers show a gradual increase in the number of harmless pores with depth. In Figures 15 and 16, the change in porosity patterns, average pore size, and median pore size of cement mortar are shown. In the early aging stages, these quantities first decrease and then increase with the duration of dry and wet cycling. In the early stage of wet and dry cycling, the porosity rapidly decreases, reaching its lowest value upon 30 wet and dry cycles, which is 13.46%. As the number of wet and dry cycles continues to increase, the porosity rises again. After 60 wet and dry cycles, the porosity reaches 14.08%. In the early stages of wet and dry cycling, the products of hydration and erosion reactions fill in the pore structure of cement mortar, leading to a denser microstructure. The thermal and microstructural analyses show that nano-metakaolin undergoes a secondary hydration reaction with the hydration products of cement, producing a large amount of C-S-H gel, hydrated calcium aluminate, and other substances. It improves the bond strength inside the cement mortar and increases its compactness. At the later stages of the dry and wet cycling, the densification of cement mortar gradually decreases, which may be related to the fact that aggressive substances begin to damage the pores of the cementitious materials. Therefore, the erosion process of chloride and sulfate ions can be divided into two stages: the first stage is the process of crystallization and precipitation of hydration and erosion products, which expand and fill the pores. The second stage is the process of cement mortar damage caused by the crystallization pressure of expansive substances acting on the pore walls [29]. In summary, improving the compactness of cement mortar and refining the pore structure of cement mortar can significantly improve the salt erosion resistance of cement mortar.

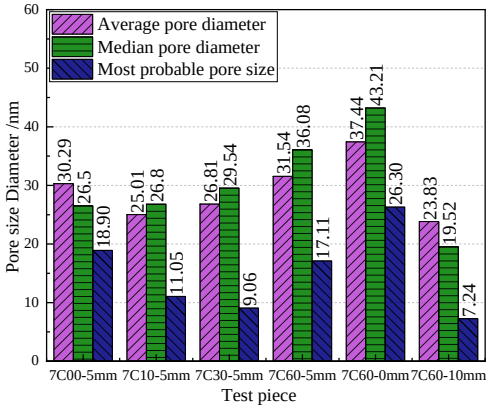

Figure 15. Distribution of mean pore diameter, most probable pore size, and total specific pore volume of cement mortar.

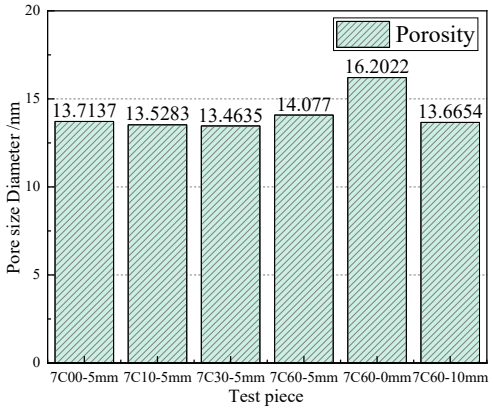

Figure 16. Porosity distribution of cement mortar.

4. Conclusions

In this paper, we studied the corrosion effect of the combined effect of chloride and sulfate ions from the groundwater in karst areas on the performance of nano-metakaolin-modified cement mortar, with an accent on the early aging stages. The selected experimental parameters were corrosion time and the duration of dry and wet cycling. For addressing long corrosion times, such as 3 or 5 years, further research is needed. The obtained results are summarized as follows:

(1) The doping of nano-metakaolin can promote the hydration of cement at an early aging stage and effectively improve its mechanical properties. At 7 d of aging, the flexural and compressive strength values of cement mortar with 1% of nano-metakaolin are increased by 10.38% and 4.41%, respectively, compared with those of ordinary cement mortar.

(2) Under the coupled effect of dry and wet cycles and chloride and sulfate erosion, the dosage of nano-metakaolin in the range of 1–5% can significantly improve the corrosion resistance of cement mortar. The flexural and compressive strength values of cement mortar with a 1% nano-metakaolin dosage are increased by 5.42 and 2.24%, respectively, compared with those of ordinary cement mortar at 7 d of aging after 30 d of wet and dry cycling.

(3) Nano-metakaolin can effectively promote the volcanic ash reaction. It generates hydration products, such as C-S-H gel, fills microcracks and micropores, improves the overall structural compactness, and enhances durability.

(4) The CH content can be used to characterize the hydration process within the cement paste. At 7 d of aging, the CH crystal content of cement mortar with a 1% nano-metakaolin dosage is increased by 32.52% compared with that of ordinary cement mortar. After 30 d of dry and wet cycling, the internal CH crystal content of the specimen with 1% of nano-metakaolin is increased by 16.44% compared with that of ordinary cement mortar. However, at 10% of added nano-metakaolin, the CH crystal content is decreased by 29.63%, showing that too much nano-metakaolin may trigger the agglomeration effect and inhibit cement hydration.

(5) Under the combined effect of wet and dry cycling and compound salt, the most abundant pore size, total specific pore volume, and porosity values in the pore structure first decrease and then increase. The pore size distribution of the same specimen narrows with the increase in depth. After 60 dry and wet cycles, the porosity of the specimens in group 7C decreased by 2.65%, and the content of harmful pores and much harmful pores decreased by 47% compared with specimens that did not undergo dry and wet cycling.

Author Contributions: Writing—original draft, J.G.; data curation, and writing—review and editing, T.Z.; investigation, F.M.; formal analysis, Y.Q.; methodology, Z.W.; resources, and funding acquisition, S.Z.; funding acquisition, H.L. All authors have read and agreed to the published version of the manuscript.

Funding: This research was funded by the Supported by the Taishan Industrial Experts Program (tscy20230660), and the National Natural Science Foundation of China (Grant No. 51908342).

Data Availability Statement: The data will be made available upon request.

Acknowledgments: The authors gratefully acknowledge the support received from the Taishan Industry Leading Talent Project, and the Natural Science Foundation of China.

Conflicts of Interest: Author Jia Guo, Tao Zheng, Fei Mou, Yang Qin and Zhi Wang was employed by the company China Construction Third Engineering Bureau Group Co., Ltd. Author Hui Li was employed by the company Zhongke Zhiyan (Shandong) Technology Development Co., Ltd. The remaining authors declare that the research was conducted in the absence of any commercial or financial relationships that could be construed as a potential conflict of interest.

References

1. Althoey, F.; Zaid, O.; Yasir, M.; Abuhussain, M.A.; Dodo, Y.; Mohamed, A. Experimental research on mechanically and thermally activation of nano-kaolin to improve the properties of ultra-high-performance fiber-reinforced concrete. *Nanotechnol. Rev.* **2024**, *13*, 20240051. [CrossRef]
2. Li, D.; Li, L.; Wang, X. Chloride diffusion model for concrete in marine environment with considering binding effect. *Mar. Struct.* **2019**, *66*, 44–51. [CrossRef]
3. Ibrahim, M.; Salami, B.A.; Khallaf, Z.; Bahraq, A.A.; Adewumi, A.A. Evaluating long-term durability of nanosilica-enhanced alkali-activated concrete in sulfate environments towards sustainable concrete development. *Constr. Build. Mater.* **2024**, *438*, 137315. [CrossRef]
4. Li, Q.; Fan, Y.; Li, X.; Shah, S.P. Effect of nano-metakaolin on the early-age fracture properties of cement mortar. *Constr. Build. Mater.* **2024**, *446*, 137922. [CrossRef]
5. Lu, C.; Gao, Y.; Cui, Z.; Liu, R. Experimental Analysis of Chloride Penetration into Concrete Subjected to Drying–Wetting Cycles. *J. Mater. Civil. Eng.* **2015**, *27*, 04015036. [CrossRef]
6. Sun, C.; Yuan, L.; Zhai, X.; Qu, F.; Li, Y.; Hou, B. Numerical and experimental study of moisture and chloride transport in unsaturated concrete. *Constr. Build Mater.* **2018**, *189*, 1067–1075. [CrossRef]
7. Pang, L.; Li, Q. Service life prediction of RC structures in marine environment using long term chloride ingress data: Comparison between exposure trials and real structure surveys. *Constr. Build Mater.* **2016**, *113*, 979–987. [CrossRef]
8. Kim, J.; Mccarter, W.; Suryanto, B.; Nanukuttan, S.; Basheer, P.; Chrisp, T. Chloride ingress into marine exposed concrete: A comparison of empirical- and physically- based models. *Cem. Concr. Comp.* **2016**, *72*, 133–145. [CrossRef]
9. Li, Y.; Wang, J.; Gao, S.; Zheng, Y. Improvement effects of nano-silica on bonding performance of polymer concrete for repairing damaged concrete. *Constr. Build Mater.* **2023**, *409*, 133768. [CrossRef]
10. Chen, X.; Ai, Y.; Wu, Q.; Cheng, S.; Wei, Y.; Xu, X.; Fan, T. Potential use of nano calcium carbonate in polypropylene fiber reinforced recycled aggregate concrete: Microstructures and properties evaluation. *Constr. Build Mater.* **2023**, *400*, 132871. [CrossRef]
11. Usanga, I.N.; Ikeagwuani, C.C.; Okafor, F.O.; Ambrose, E.E. Exploration of calcined clays and nanoclays as a potential construction material for sustainable development: A comprehensive and state-of-the-art review. *Road Mater. Pavement Des.* **2024**, 1–34. [CrossRef]
12. Dalla, T.P.; Tragazikis, K.I.; Exarchos, A.D.; Dassios, K.G.; Barkoula, N.M.; Matikas, T.E. Effect of Carbon Nanotubes on Chloride Penetration in Cement Mortars. *Appl. Sci.* **2019**, *9*, 1032. [CrossRef]
13. Konsta-Gdoutos, S.M.; Batis, G.; Danoglidis, A.P.; Zacharopoulou, A.K.; Zacharopoulou, E.K.; Falara, M.G.; Shah, S.P. Effect of CNT and CNF loading and count on the corrosion resistance, conductivity and mechanical properties of nanomodified OPC mortars. *Constr. Build. Mater.* **2017**, *147*, 48–57. [CrossRef]
14. Dalla, P.T.; Tragazikis, I.K.; Trakakis, G.; Galiotis, C.; Dassios, K.G.; Matikas, T.E. Multifunctional Cement Mortars Enhanced with Graphene Nanoplatelets and Carbon Nanotubes. *Sensors* **2021**, *21*, 933. [CrossRef]
15. Chen, K.-Y.; Xia, J.; Wang, S.-Q.; Wu, R.-J.; Min, W.-L.; Wei, J.-Y.; Hou, D.-S.; Mu, S. Insights on the chloride adsorption stability in cement mortar under current field and sulfate attack: From experiments to molecular dynamics simulation. *Cem. Concr. Compos.* **2024**, *146*, 105375. [CrossRef]

16. Maohua, Z.; Danan, M.; Jia, H.; Yue, H. Sulfate corrosion resistance of foundation concrete with nano-particles. *Mag. Civ. Eng.* **2023**, *119*, 11901.
17. Mokhtar, M.M. Evaluating the physico-mechanical performance of cement mortar reinforced with metakaolin/graphene oxide dual nano-additives. *Innov. Infrastruct. Solut.* **2024**, *9*, 75. [CrossRef]
18. Raza, A.; Ahmed, M.; Khan, Q.U.Z.; Azab, M.; Arshad, M. Effectiveness of using nanoparticles in green composites: A scientometric analysis of fresh, mechanical, durability, and microstructural features. *Constr. Build. Mater.* **2023**, *402*, 133077. [CrossRef]
19. Malayali, A.B.; Venkatesh, R.; Alharbi, S.A.; Kalam, M. Hybridization of concrete by the inclusions of kaolin, alumina and silica fume: Performance evaluation. *Heliyon* **2024**, *10*, e30674. [CrossRef]
20. Niu, X.; Feng, G.; Han, Y.; Liu, Q.; Xue, G.; Cui, J.; Song, C. Synergistic effect of surfactant and chlorine salt on dispersion of nano-SiO_2 and performance of cement-based grout containing a large amount of bentonite. *Cem. Concr. Compos.* **2022**, *131*, 104587. [CrossRef]
21. Shilar, F.A.; Ganachari, S.V.; Patil, V.B. Advancement of nano-based construction materials-A review. *Constr. Build. Mater.* **2022**, *359*, 129535. [CrossRef]
22. Feng, Z.; Chen, H.; Wang, F.; Hu, H.; Xu, Z.; Yao, X. Corrosion damage of bridge pile foundation under dry-wet circulation in strong salt marsh. *J. Traffic Transp. Eng.* **2023**, *23*, 156–167.
23. *GB/T17671-2021*; Test Method of Cement Mortar Strength (ISO Method). The State Administration for Market Regulation of China: Beijing, China, 2021.
24. Ali, T.; Zaid, O.; Qureshi, M.Z. Impact of Mechanical and Thermal Treatment of Kaolin Clay on the Engineering Properties of Concrete. *Arab. J. Sci. Eng.* **2024**, *50*, 1991–2007. [CrossRef]
25. Ma, Q.; Li, Y.; Liu, J.; Ying, H.; Han, H.; Chen, X. Enhanced dispersing properties of kaolin due to high-strength kneading process. *Appl. Clay Sci.* **2024**, *247*, 107218. [CrossRef]
26. Wilson, W.; Gonthier, J.N.; Georget, F.; Scrivener, K.L. Insights on chemical and physical chloride binding in blended cement pastes. *Cem. Concr. Res.* **2022**, *156*, 106747. [CrossRef]
27. Rasheed, P.A.; Nayar, S.K.; Barsoum, I.; Alfantazi, A. Degradation of concrete structures in nuclear power plants: A review of the major causes and possible preventive measures. *Energies* **2022**, *15*, 8011. [CrossRef]
28. Al-Adhadh, A.R.; Daud, N.N.N.; Yusuf, B.; Al-Rkaby, A.H. Supplementary cementitious materials in sandy soil improvement: A review. *J. Build. Pathol. Rehabil.* **2024**, *9*, 138. [CrossRef]
29. Luo, S.; Wei, J.; Xu, W.; Chen, Y.; Huang, H.; Hu, J.; Yu, Q. Design, preparation, and performance of a novel organic–inorganic composite coating with high adhesion and protection for concrete. *Compos. Part B Eng.* **2022**, *234*, 109695. [CrossRef]